Special Collection

Steric Effects on the Thermal Processes of Hemithioindigo Based Molecular Motor Rotation

Ludwig A. Huber,[a] Stefan Thumser,[a] Kerstin Grill,[a] David Voßiek,[a] Nicolai N. Bach,[b] Peter Mayer,[a] and Henry Dube*[b]

In memory of François Diederich

Abstract: Tuning the thermal behavior of light driven molecular motors is fundamentally important for their future rational design. In many molecular motors thermal ratcheting steps are comprised of helicity inversions, energetically stabilizing the initial photoproducts. In this work we investigated a series of five hemithioindigo (HTI) based molecular motors to reveal the influence of steric hindrance in close proximity to the rotation axle on this process. Applying a high yielding synthetic procedure, we synthesized constitutional isomeric derivatives to distinguish between substitution effects at the aromatic and aliphatic position on the rotor fragment. The kinetics of thermal helix inversions were elucidated using low temperature ^{1}H NMR spectroscopy and an *in situ* irradiation technique. In combination with a detailed theoretical description, a comparative analysis of substituent effects on the thermal helix inversions of the rotation cycle is now possible. Such deeper understanding of the rotational cycle of HTI molecular motors is essential for speed regulation and future applications of visible light triggered nanomachines.

Introduction

For the past two decades the field of light driven molecular motors[1] has been expanding vividly.[1b,c,2] Recently synchronous motion,[3] the transduction of directional motion at the molecular[4] or macroscopic scale,[5] high level control of motor functionality,[6] applications in catalysis,[7] or the exploration of alternative motor concepts, both experimentally and theoretically,[2a,c,h,j,l,8] have been achieved. Yet, applications in biology related fields[9] are still limited by the need for using high energy UV light for most molecular motor operations. Employing indigoid chromophores[10] as chemical core structures, we have been able to shift addressability of molecular switches and motors into the region of less energetic visible light. Three different types of molecular motors have been developed by our group so far using hemithioindigo (HTI)[2j,10b,11] as structural platform. The first type operates similar to the classical Feringa motor in four different steps in which two photoisomerization reactions are intersected by thermal helix inversion steps.[2e–g,i,4a] The second type of motor operates in three steps each of which is light driven and thus thermal ratcheting steps are omitted.[2h] The third type allows a more complex directional motion to be realized where a figure eight shape is followed in four distinct steps.[2j]

The first type of HTI based molecular motors is able to perform a fully directional and repetitive rotation around the central double bond upon visible light input. To decipher the whole rotational cycle with the high resolution power of NMR spectroscopy we increased the steric hindrance in close proximity to the central double bond.[2g] The resulting higher ground state barriers for thermal helix inversions enabled a direct experimental observation of the sequential population of all four ground state intermediates and thus of the unidirectionality. Later studies with ultrafast spectroscopy enabled also a comprehensive mechanistic picture of the excited state processes in the original HTI motor[2f] and in a series of three HTI motors with increased steric hindrance at one position of the rotor fragment.[12] In the present work we used our previously developed synthetic methodology[2g] to synthesize two new and constitutional isomeric HTI motor derivatives in order to investigate the influence of sterically demanding substituents at different sides of the rotor fragment. With these new derivatives in hand a series of five HTI motors **1**–**5** with different steric hindrance in close proximity to the photoisomerizable double bond could now quantitatively be compared with respect to their thermal ratcheting processes.

[a] Dr. L. A. Huber, S. Thumser, K. Grill, D. Voßiek, Dr. P. Mayer
Department für Chemie and
Munich Center for Integrated Protein Science CIPSM
Ludwig-Maximilians-Universität München
81377 Munich (Germany)

[b] N. N. Bach, Prof. Dr. H. Dube
Department of Chemistry and Pharmacy
Friedrich-Alexander-Universität Erlangen-Nürnberg
Nikolaus-Fiebiger-Str. 10, 91058 Erlangen (Germany)
E-mail: henry.dube@fau.de

Supporting information for this article is available on the WWW under https://doi.org/10.1002/chem.202100950

Special Collection This article belongs to a Joint Special Collection dedicated to François Diederich.

Results and Discussion

General setup of the HTI motor comparison

The unidirectional rotation mechanism of selected first type HTI motors has been explored previously by variable temperature ^{1}H NMR spectroscopy as well as multiscale broadband transient absorption measurements and resembles the rotation cycle followed by overcrowded alkenes.[2g] Figure 1 depicts the general energy profile of their light powered rotation and the corresponding structures of the four different ground state minima populated during this process in a repetitive sequence. These structures all contain a stable sulfoxide stereocenter and differ by the configuration of the double bond and the helical twist of the rotor part relative to the stator part. Their individual stereo configuration is given in Figure 1 together with the more convenient labeling **A** to **D**, which is used in the following.

Irradiation of *E*-configured isomer **A** leads to photoisomerization of the central double bond and population of *Z*-configured isomer **B**. In the next step isomer **B** converts to the thermodynamically more stable isomer **C** in a thermal helix inverting step. This concludes the first unidirectional 180° rotation. A photoinduced *Z*/*E* isomerization of isomer **C** to the metastable isomer **D** is again followed by a thermal helix inversion, which regenerates isomer A as the starting point of the cycle. In sum a repetitive rotary motion occurs as long as light and sufficient thermal energy is available. All HTI-based motor derivatives **1**–**5** exhibit higher energy barriers ($\Delta G^{\neq}$ = 13.10–15.39 kcal/mol) for the thermal **D** to **A** helix inversions, which facilitates direct observation of this step by low temperature ^{1}H NMR spectroscopy. Thermal **B** to **C** isomerizations are accompanied by lower energy barriers, which impeded direct observation of this process for the first generation of this type of HTI based molecular motors. After synthesizing sterically crowded derivatives, exhibiting significantly higher barriers for their thermal helix inversions, the elusive **B** to **C** ground state process could be observed directly by low temperature ^{1}H NMR spectroscopy.[2g] To this end different aliphatic groups were introduced at the aromatic position of the rotor fragment in close vicinity to the central double bond. In this work we compare the formerly studied derivatives **1**, **2**, and **5**, which vary in the steric hindrance of substituents at the aromatic part of the rotor fragment with two newly synthesized derivatives **3** and **4** (Figure 1). The new derivatives are constitutional isomers of each other and steric hindrance is varied systematically on both sides, e.g. the aromatic position (R^1) and the aliphatic quaternary carbon (R^3) of the rotor fragment. This also allows for the first time to probe the influence of varied sterics at the aliphatic quaternary carbon center of the rotor fragment and at the same time reveals important design criteria for conscious adjustment of motor performance in the future.

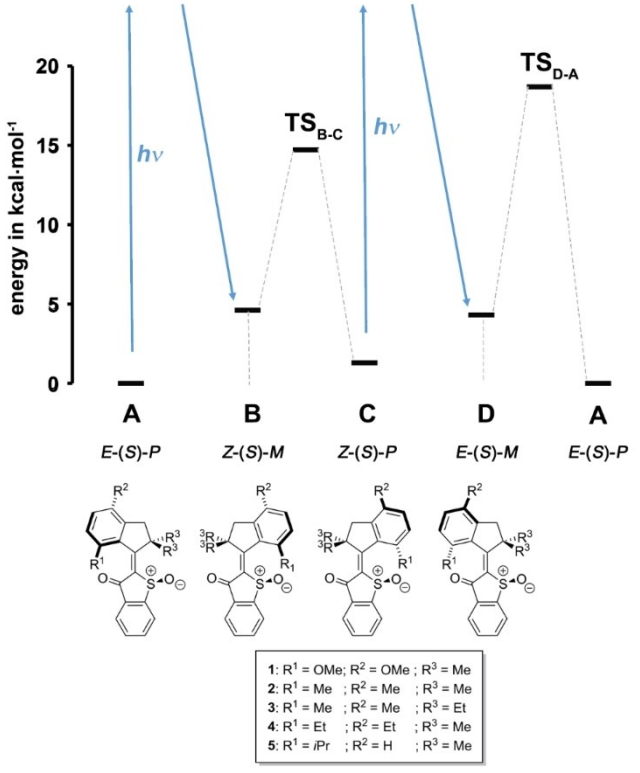

Figure 1. General energy profile of HTI molecular motors **1**–**5** with assignment of the stereo configurations. One full rotation cycle consists of two light induced photoisomerizations (indicated by blue arrows), which are separated by two thermal helix inversions in the ground state. The former convert isomer **A** to **B** and isomer **C** to **D**. The latter convert isomer **B** to **C** (ground state energy barrier $\Delta G^{\neq}_{B\text{-}C}$ corresponding to the transition state $TS_{B\text{-}C}$) and isomer **D** to **A** (ground state energy barrier $\Delta G^{\neq}_{D\text{-}A}$ corresponding to the transition state $TS_{D\text{-}A}$). All derivatives exhibit lower energy barriers for thermal **B** to **C** helix inversions rendering the helix inversion from **D** to **A** the rate limiting step in terms of thermal energy.

Synthesis

The synthesis of derivatives **1**, **2**, and **5** was previously reported.[7a,b] Derivatives **3** and **4** were synthesized following the same protocol as used for derivatives **2** and **5** (Figure 2; for full details of the synthesis see the Supporting Information). A nucleophilic addition of an *in situ* generated lithium acetylide species Li-**6** to indanones **7** and **8** bearing different substituents delivers the corresponding propargylic alcohols in 75% yield for derivative **9** and 89% for derivative **10**. An acid catalyzed *Meyer Schuster* rearrangement and consecutive oxidation with perborate yielded intermediate enone sulfoxides **13** and **14**. The sulfoxides are transformed *in situ* to reactive chlorosulfonium species by addition of oxalyl chloride, which underwent a multistage ring closing reaction towards the corresponding HTIs **15** and **16**. Final oxidation delivers motor derivative **3** with 79% and derivative **4** with 69% overall yields, when starting from the isolated propargylic alcohols. This protocol also works without purification of synthetic intermediates and excellent overall yields of 59% for **3** and 61% for **4** could be achieved for these four-step sequences. Racemic crystals suitable for structural analysis were obtained for isomers **A** and **C** of HTI motor **3** (Figure 2).

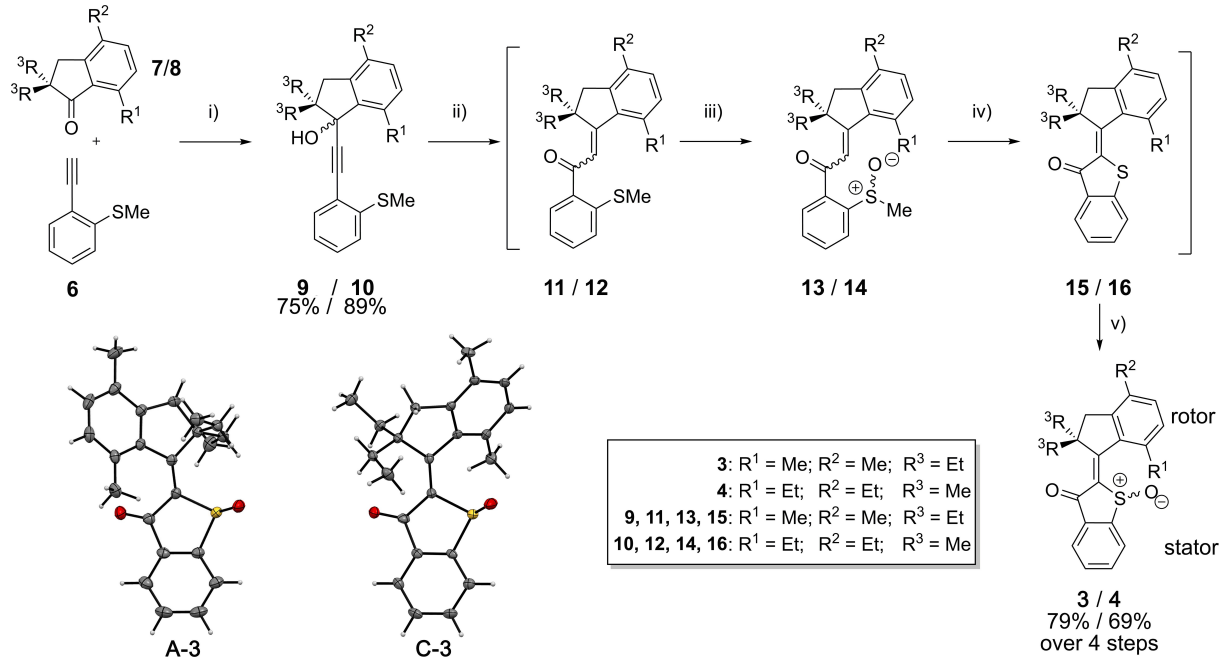

Figure 2. Synthesis of motor derivatives **3** and **4**. i) *n*BuLi, THF, −78–0 °C, 75% for **9** and 89% for **10**; ii) H_2SO_4, THF, 23 °C; iii) Sodium perborate, AcOH, 23 °C; iv) Oxalyl chloride, CH_2Cl_2, −50 °C; v) Sodium perborate, AcOH, 23 °C, 3 h, 79% for **3** and 69% for **4** over 4 steps. Overall yields of 59% for motor **3** and 61% for motor **4** were achieved. Structures in the crystalline state could be obtained for racemic **C-3** and **A-3**. Structures with (*S*) configuration are shown exemplarily.

Kinetic measurements and light powered unidirectional rotations of 3 and 4

The Gibbs energy of activation $\Delta G^{\ddagger}_{D\text{-}A}$ of the thermal **D** to **A** helix inversion for motors **1**–**5** as well as $\Delta G^{\ddagger}_{B\text{-}C}$ for the **B** to **C** helix inversion of motor **5** were measured by low temperature ^{1}H NMR spectroscopy using an *in situ* irradiation technique. To this end motors **1**–**5** were dissolved in CD_2Cl_2 or in a 4/1 mixture of CD_2Cl_2/CS_2 and subsequently NMR samples were cooled to −70 to −105 °C. At suitable low temperatures, irradiation with blue light leads to accumulation of the metastable states **B** (only visible in the NMR spectra for HTI motor **5**) and **D** (visible for all HTI motors). Their thermal decays in the dark were followed by recording a series of NMR spectra over the course of seconds to several hours, depending on the specific rate constants of the reaction. Kinetic analysis confirmed the helix inversions as first order reactions allowing to determine the $\Delta G^{\ddagger}$ values for these processes. Due to very fast thermal relaxation the corresponding $\Delta G^{\ddagger}_{B\text{-}C}$ values for thermal **B**-**1** to **C**-**1** and **B**-**2** to **C**-**2** conversions were obtained by time resolved absorption spectroscopy at 22 °C in CH_2Cl_2 solution using a multiscale broadband setup covering 12 orders of magnitude in time, as previously reported.[12]

The experimental data obtained for derivatives **3** and **4** evidence unidirectional motor behavior analogous to the previously studied HTI motor derivatives **1**, **2**, and **5**. The photoreactions of pure isomers **C**-**3** and **C**-**4** at −80 °C were followed by recording a series of ^{1}H NMR spectra during 470 nm illumination. The irradiation leads to build up of a new set of signals in each case, which could be assigned to the **D**-**3** and **D**-**4** isomers, respectively. The thermal decay of isomers **D**-**3** and **D**-**4** was followed after switching off the light at low temperatures in the dark. Only isomers **A**-**3** and **A**-**4**, respectively were repopulated during this process. Thermal annealing of the solutions to ambient temperature and subsequent re-cooling to low temperature directly showed conversion of at least 95% of **D**-**3** and **D**-**4** to **A**-**3** and **A**-**4**, respectively as determined by the accuracy of ^{1}H NMR spectroscopy. Therefore, complete unidirectionality of 180° double bond rotation leading from isomeric state **C** to **A** could be shown directly and unambiguously for the new HTI motors **3** and **4**. The corresponding energy barriers were found to be $\Delta G^{\ddagger}_{D\text{-}A}$ = 14.30 kcal/mol for motor **3** and $\Delta G^{\ddagger}_{D\text{-}A}$ = 15.43 kcal/mol for motor **4**.

The photoreactions of pure **A**-**3** and **A**-**4** were followed at −80 °C and −70 °C, respectively using ^{1}H NMR spectroscopy. It could be observed, that immediately after irradiation began, the known set of signals of isomers **C**-**3** and **C**-**4** started to build up. Only afterwards the signals of isomers **D**-**3** and **D**-**4** also began to rise until a steady state isomer composition was reached in the photostationary state (pss). These measurements can be interpreted as follows: Photoisomerization of isomer **A** leads to a very short-lived isomer **B**, which cannot be observed at −70 to −80 °C with ^{1}H NMR spectroscopy. Fast thermal conversion of **B** leads to isomer **C**, which was observed as the apparent first product formed during the irradiation experiment. Isomer **C** is accumulating due to the initial high concentration of isomer **A**, which is the predominant photon absorbing species at this time point of the experiment. As soon as isomer **C** concentration is high enough in the irradiated

sample solution, light induced conversion of isomer **C** leads to detectable amounts of the next intermediate **D** of the rotation cycle, which can be seen in the decrease of isomer **C** and the increase of **D** at a later point of time of the experiment. Accumulation of isomer **D** occurs, because low temperature prevents its fast decay, until the pss between **C** and **D** is reached. Similar to the original first generation HTI motor a contradictory behavior is observed with isomer **C** seemingly attending two different photoequilibria depending on the starting point. If starting from **C** itself a photo equilibrium with thermally stable **D** is established, while starting from **A** the same stable isomer **C** seems to be the photoproduct. In reality, the latter does not represent a true photoequilibrium between **A** and **C** but in fact a mixed process of **A** to **B** photo-isomerization and instant thermal helix inversion from **B** to **C**. This behavior gives indirect evidence, that isomer **B** is thermally very labile and is therefore not observed during the NMR experiment, but instead only its thermal conversion product **C**.

Discussion

To obtain comprehensive and quantitative insights into the influence of different substitution patterns on the thermal ratcheting steps of HTI based molecular motors, we compare all five motors **1**–**5** in the following (Figure 3). The experimentally determined Gibbs energies of activation $\Delta G^{\ddagger}$ values as well as ΔG values of individual states **A** to **D** are summarized in Figure 3b (experimental values) and c (values derived from the theoretical description). Within the whole series, motors **1**, **2**, **4**, and **5** bear substituents with increasing steric demand at the aromatic part of the rotor fragment. A considerable increase of the energy barrier for the thermal **D** to **A** helix inversion of 1.94 kcal/mol is observed, when comparing the methoxy-substituted derivative **1** to the methyl-substituted derivative **2** in this sub-series measured in pure CD_2Cl_2. Changing the methyl-substituent in **2** to an ethyl-substitution in derivative **4** increases $\Delta G^{\ddagger}_{D\text{-}A}$ by another 0.39 kcal/mol in pure CD_2Cl_2 solutions. Comparison of motor **4** and **5**, which represent further steric increase at the aromatic position, is possible for the solvent mixture CD_2Cl_2/CS_2 (4/1). The decay of the metastable isomers **D** is slightly faster in case of motor **4** with a $\Delta G^{\ddagger}$ difference of 0.11 kcal/mol. At this point the influence of CS_2 addition to the CD_2Cl_2 solvent can also be assessed for the thermal **D** to **A** helix inversion of **4** showing a slight acceleration in the mixed solvent by 0.15 kcal/mol. Thus, it can be stated, that increased steric hindrance at the aromatic position in the series of **1**, **2**, **4**, **5** leads to significant deceleration of the thermal **D** to **A** conversion.

When looking at the **B** to **C** helix inversion even larger effects are observed for substitution changes at the aromatic side of the rotor fragment, that is within the sub-series **1**, **2**, (**4**), and **5**. Exchange of the methoxy-group (motor **1**) by a methyl-group (motor **2**) leads to an increase of $\Delta G^{\ddagger}_{B\text{-}C}$ of 3.74 kcal/mol. Changing the methyl-group to an *iso*-propyl group (motor **5**) further increases the barrier by another 2.49 kcal/mol. Taking into account the theoretical description, the change from a methyl group (motor **2**) to an ethyl group (motor **4**) leads to an intermediate increase of $\Delta G^{\ddagger}_{B\text{-}C}$ of 1.85 kcal/mol. Comparing the range of experimentally determined energy changes induced by increasing steric hindrance on the aromatic side from a methoxy to an *iso*-propyl substituent (i.e., an increase of 6.23 kcal/mol for $\Delta G^{\ddagger}_{B\text{-}C}$ and a corresponding increase of 2.29 kcal/mol for $\Delta G^{\ddagger}_{D\text{-}A}$), it can be concluded that the thermal **B** to **C** helix inversion is more sensitive to structural changes at the aromatic part of the rotor than the **D** to **A** helix inversion.

In motors **2** and **3** the steric demand is increased at the aliphatic quaternary carbon center (R^3) on the rotor fragment, while sterics at the aromatic side are kept the same. Comparing derivatives **2** and **3** therefore allows to decipher whether increase in the steric demand at the quaternary carbon center is also effective for increasing the energy barriers for the thermal helix inversion steps. Thus, the effects of increasing sterics on

a)

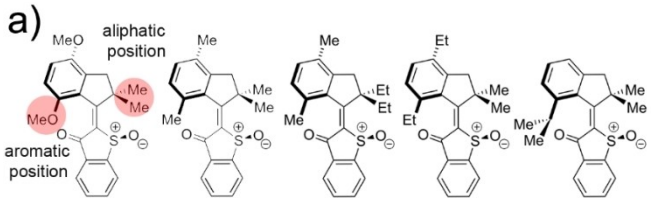

b)

motor	A	B	$\Delta G^{\ddagger}_{B\text{-}C}$	C	D	$\Delta G^{\ddagger}_{D\text{-}A}$
1	0.81[4]	>1.73[1]	5.76[1]	0.00[4]	>1.73[1]	13.10[3] 13.33[1]
2	0.00[4]	>1.73[1]	9.50[1]	1.29[4]	>1.13[2]	14.38[2] 15.04[5]
3	0.00[4]	-	-	0.87[4]	>1.13[3]	14.30[3] 14.64[5]
4	0.00[4]	-	<11.30[2]	1.11[4]	>1.19[3]	15.43[3] 15.28[2]
5	0.00[4]	>1.73[1]	11.30[2] 11.99[1]	1.07[4]	>1.19[2]	15.39[2]

c)

motor	A	B	$\Delta G^{\ddagger}_{B\text{-}C}$	C	D	$\Delta G^{\ddagger}_{D\text{-}A}$
1	0.81	3.35	5.53	0.00	4.32	13.46
2	0.00	4.61	10.10	1.41	4.32	15.17
3	0.00	5.29	8.13	0.99	3.69	14.21
4	0.00	3.87	11.95	1.24	4.30	15.80
5	0.00	3.56	13.56	1.10	4.25	15.77

Figure 3. Energy comparison between HTI based molecular motors **1**–**5** with increased steric hindrance. The corresponding experimentally determined and calculated $\Delta G^{\ddagger}$ and ΔG values are given in kcal/mol. a) Structures of the HTI based molecular motors are depicted as (*S*) configured isomer **A**. b) Experimentally determined energy values obtained either by variable temperature ^{1}H NMR spectroscopy or by applying time resolved transient absorption measurements. [1] Values determined in CH_2Cl_2 at 22 °C by transient absorption measurements. [2] Measured in CD_2Cl_2/CS_2 (4/1 ratio) by low temperature ^{1}H NMR spectroscopy ($\Delta G^{\ddagger}_{D\text{-}A}$ **2**: −80 °C; **4**, **5**: −70 °C and $\Delta G^{\ddagger}_{B\text{-}C}$ **4**, **5**: −105 °C). [3] Measured in CD_2Cl_2 by low temperature ^{1}H NMR spectroscopy (**1**: −90 °C; **3**: −80 °C; **4**: −70 °C). [4] Measured in toluene-d_8 (**1**, **3**, **4** and **5**) or xylene-d_{10} (**2**) at 100 °C by ^{1}H NMR spectroscopy. [5] Thermal decay of metastable isomers **D** monitored simultaneously in an equimolar CD_2Cl_2 solution of **2** and **3** at −80 °C. c) Calculated energy values of the ground state energy profile are provided on the MPW1 K/6-311G(d,p) level of theory and are given in kcal/mol.

both sides of the rotor fragment can be probed independently from each other. Moreover, since derivative **3** is a constitutional isomer of derivative **4**, it can be derived, which position dominates the energy barriers of thermal helix inverting steps by comparing all three isomers **2**, **3**, and **4**. The obtained results are summarized in Figure 4.

For derivatives **2** and **3** the kinetics of thermal **D** to **A** conversion are very similar. Therefore the kinetics of this process were measured in a mixture of **2** and **3** in roughly 1:1 ratio at −80 °C in CD_2Cl_2 solution (Figure 4b and c). From this experiment it becomes evident (even by visual inspection) that thermal decay of **D-3** ($\Delta G^{\ddagger}_{D\text{-}A} = 14.30$ kcal/mol in CD_2Cl_2 and 14.64 kcal/mol in CD_2Cl_2 in the presence of 1 equiv. of **3**) is indeed faster than the decay of **D-2** ($\Delta G^{\ddagger}_{D\text{-}A} = 14.38$ kcal/mol in CD_2Cl_2/CS_2 (4/1) and 15.04 kcal/mol in CD_2Cl_2 in the presence of 1 equiv. of **2**). The $\Delta G^{\ddagger}_{D\text{-}A}$ values for **2** and **3** are both smaller than the value for derivative **4** (15.43 kcal/mol in in CD_2Cl_2 and 15.28 kcal/mol in CD_2Cl_2/CS_2 (4/1)). Contrary to the decelerating

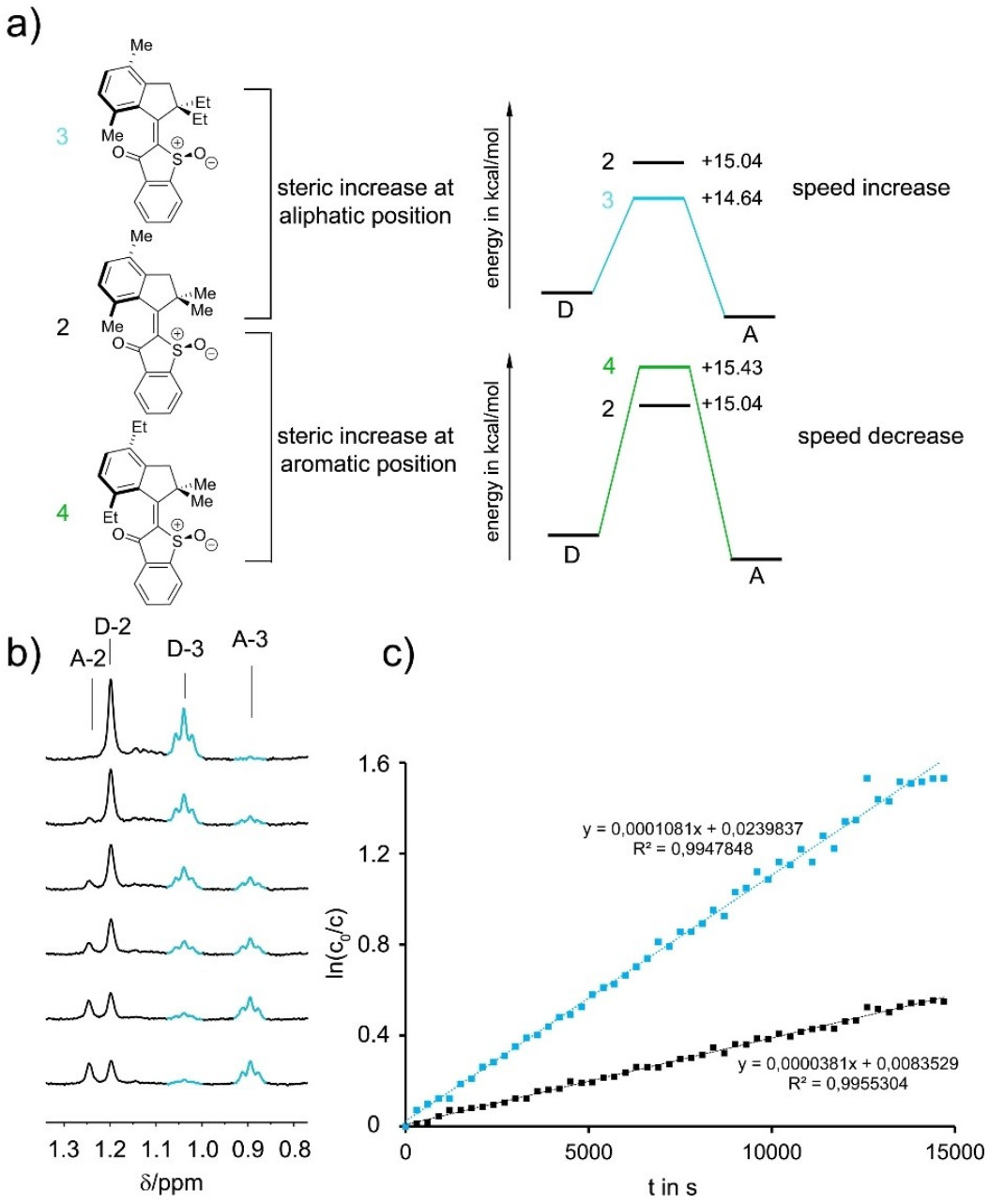

Figure 4. Comparison of the thermal helix inversions for motor derivatives **2**, **3** and **4**. a) Steric increase at the aliphatic quaternary carbon center leads to a decrease of $\Delta G^{\ddagger}_{D\text{-}A}$ from 15.04 kcal/mol for motor **2** to 14.64 kcal/mol for motor **3**. Increased sterics at the aromatic position leads to an increase of $\Delta G^{\ddagger}_{D\text{-}A}$ from 15.04 kcal/mol to 15.43 kcal/mol. b) Selected signals of the ^{1}H NMR spectra, recorded during the thermal decay of isomers **D-2** and **D-3** in a mixed solution with equimolar concentration of motor **2** and **3**. The decay of **D-3** (turquoise) is faster than the decay of **D-2** (black). c) First order kinetic analysis of thermal **D** to **A** conversion for motors **2** and **3** derived from the kinetics experiment of a 1:1 mixture of both motors. Faster isomer **D** decay for motor **3** than for motor **2** is observed.

effects of increasing sterics at the aromatic positions, steric increase at the aliphatic quaternary carbon center does in fact lead to a decrease of the energy barrier of thermal **D** to **A** helix inversion and thus acceleration of this process. The corresponding $\Delta G^{\ddagger}_{B\text{-}C}$ values for the thermal helix inversion from isomers **B** to **C** could not be assessed experimentally for the new derivatives **3** and **4** and thus steric influences cannot be compared quantitatively at the aliphatic side of the rotor fragment.

From the experimental kinetic data it is not possible to conclude whether changes in the ground state energies, for example, changes of the Gibbs free energy ΔG of the metastable isomers **B** and **D**, are responsible for the varying energy barriers of thermal helix inversions or if the transition state energies $\Delta G^{\ddagger}$ are directly influenced themselves by the structural changes. The group of Feringa already reported about both phenomena,[9] rendering a prediction of the effects of increased steric hindrance in close proximity to the rotation axle difficult. Experimental access to the relative ground state Gibbs free energies ΔG is hampered in HTI motors because of the large energy differences between metastable and stable isomers, leading to exclusive population of the stable isomers **A** and **C** under equilibrium conditions.

Theoretical description

To gain further insights into the energy-landscape changes associated with the different substitutions in HTI motors **1**–**5**, a comprehensive theoretical assessment on the MPW1K/6-311G (d,p) level of theory was performed. The theoretical description also delivers further information on experimentally not accessible key features of the ground state energy profile. Detailed information about the theoretical description of motor **3** and **4** can be found in the Supporting Information. Theoretical data for derivatives **1**, **2**, and **5** on the same level of theory can be found in references.[2e,g] In Figure 5 the obtained calculated energies for motors **2**–**5** are summarized.

For all derivatives **1**–**5** four ground state minima **A**–**D** were found as well as two energetically low lying transition states (TS), associated with the two helix inverting processes **D** to **A** and **B** to **C**. For all optimized structures frequency analyses confirmed them to be stationary points. One imaginary frequency was obtained for the transition states showing that they are first order saddle points on the hyper-potential energy surface.

Considering the minimum structures **A** and **C**, the theoretical description reproduces very well the experimentally observed stability order, which is **C** < **A** for motor **1** and **A** < **C** for all other motors **2**–**5**. Likewise absolute energies compare well between theory and experiment. It was previously reported, that the experimental $\Delta G^{\ddagger}_{D\text{-}A}$ (and $\Delta G^{\ddagger}_{B\text{-}C}$) values of motors **1**, **2**, and **5** are also in good agreement with the theoretically obtained values.[7] The corresponding theory values for $\Delta G^{\ddagger}_{D\text{-}A}$ of motor derivatives **3** and **4** were likewise found to be in good agreement with the experimental values measured in solution.

The calculated ground state minima **B** and **C** and the corresponding transition state energies of motor derivatives **2**, **4**, and **5** exhibit direct correlations with increasing steric bulk of the aromatic substituent on the rotor fragment, which is illustrated in Figure 5a. Increasing the steric hindrance from derivative **2** to **5** leads to a noticeable decrease of the ground state minimum energies of isomers **B** and **C**, with larger effect on the former. At the same time increased steric hindrance leads to significantly increased energies of the transition state $TS_{B\text{-}C}$, connecting the **B** and **C** minima. The calculated increased barrier $\Delta G^{\ddagger}_{B\text{-}C}$ within this series is therefore a direct consequence of the sum of both trends. Although the observed stabilization of the metastable isomer **B** with increasing steric bulk at the aromatic position appears counterintuitive it

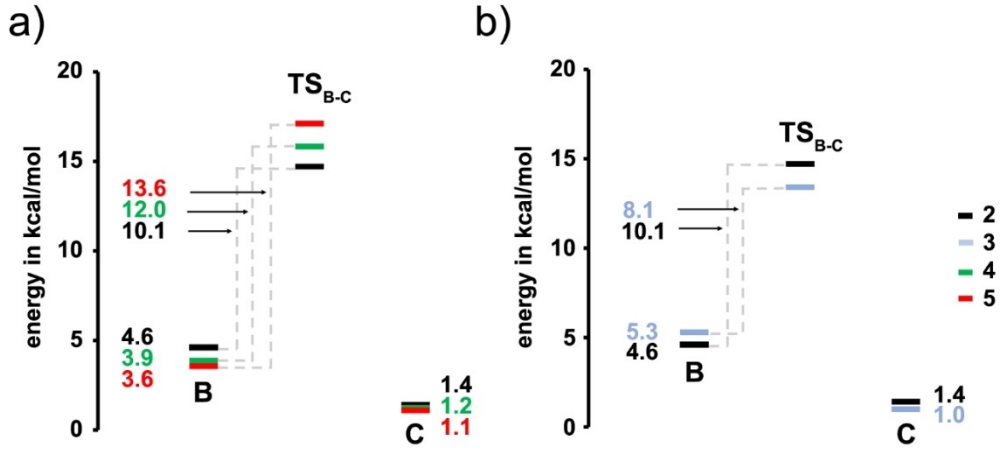

Figure 5. Ground state energy profiles of the of motors **2** (black), **3** (blue), **4** (green), and **5** (red) describing the thermal **B** to **C** isomerization as calculated on the MPW1K/6-311G(d,p) level of theory. Free enthalpies are given in kcal/mol. a) Comparison of derivatives **2**, **4** and **5**, which represent a series of increased steric bulk at the aromatic position. A direct correlation is observable. Increased steric hindrance leads to noticeably decreased minimum energies for isomers **B** resulting in increased barriers for the helix inversion. b) Comparison of derivatives **2** and **3**. A possible explanation for the theoretically predicted decreased barrier for thermal **B** to **C** helix inversion is the calculated destabilization of isomer **B**-**3**.

provides an explanation for the measured $\Delta G^{\ddagger}_{B\text{-}C}$ trend in the experiments.

The experimentally determined energies $\Delta G^{\ddagger}_{B\text{-}C}$ for motors **2** and **5** are consistent with the theoretical description but experimental data for derivative **4** are missing because of the apparently low energy barrier hampering NMR analysis. The theoretical description of derivative **3** predicts a noticeable decrease of the energy $\Delta G^{\ddagger}_{B\text{-}C}$ and a higher minimum energy ΔG of isomer **B** as compared to **2**. This is again consistent with the corresponding energy $\Delta G^{\ddagger}_{D\text{-}A}$ calculated for the **D** to **A** conversion, which was also confirmed experimentally by the direct comparison experiment in a 1:1 mixture of motors **2** (less sterical hindrance $\Delta G^{\ddagger}_{D\text{-}A} = 15.17$ kcal/mol) and **3** (increased sterical hindrance $\Delta G^{\ddagger}_{D\text{-}A} = 14.21$ kcal/mol). Future time resolved experiments have to be carried out in order to verify the theoretical prediction for the **B** to **C** conversion of motor **3**. If the theory will be confirmed, a destabilization of the ground state energy of metastable isomer **B** could be indeed responsible for the lowered barrier of the thermal **B** to **C** conversion despite an increase in steric hindrance in the case of derivative **3**.

Conclusion

In conclusion we have studied a series of five HTI molecular motors quantitatively with respect to the influences of different steric substitution effects on their thermal ratcheting motions. It could be shown, that increased steric hindrance at the aromatic position of the rotor fragment is decelerating thermal helix inversion, which interconverts isomer **D** to **A**. On the contrary increased sterics at the aliphatic quaternary carbon center, as it was shown for derivative **3**, leads to faster thermal **D** to **A** conversion. As the thermal speed limit is dictated by the highest energy barrier of the whole rotation cycle, both positions are suitable for maximum speed tuning of HTI based molecular motors. Decreasing the steric bulk at the aromatic position and increasing it at the quaternary carbon position would therefore be most effective in accelerating the thermal motor steps significantly. An even more pronounced sensitivity towards steric increase at the aromatic position is observed for the **B** to **C** helix inversion, which is however a much faster process as compared to the **D** to **A** conversion. Theoretical calculations generally reproduced the ground state energy profiles of all HTI motors well. Similar to the thermal **D** to **A** conversion, theory also predicts a decrease of the thermal **B** to **C** helix inversion of motor **3**, despite an increase of steric hindrance near the rotation axle, which will be tested experimentally by time resolved spectroscopy in the future. Taken together, this study delivers quantitative data suitable for the rational design of novel HTI based motors with specific maximum rotational speeds, that can be optimized for future applications in catalysis, molecular mechanics, or integrated molecular machinery.

Experimental Details

Full experimental details of synthesis, motor analysis, photoisomerization reactions, thermal reactions, photophysical properties, crystal structures, NMR of intermediates and theoretically obtained geometries can be found in the Supporting Information.

Deposition Number(s) 2070299 (for **A-3**), and 2070300 (for **C-3**) contain(s) the supplementary crystallographic data for this paper. These data are provided free of charge by the joint Cambridge Crystallographic Data Centre and Fachinformationszentrum Karlsruhe Access Structures service www.ccdc.cam.ac.uk/structures.

Acknowledgements

H.D. thanks the "Fonds der Chemischen Industrie" for a Liebig fellowship (Li 188/05) and the Deutsche Forschungsgemeinschaft (DFG) for an Emmy-Noether fellowship (DU 1414/1-2). K.G. thanks the "Fonds der Chemischen Industrie" for a Chemiefonds fellowship (Do 199/53). We further thank the Deutsche Forschungsgemeinschaft (SFB 749, A12) and the Cluster of Excellence'Center for Integrated Protein Science Munich' (CIPSM) for financial support. Open access funding enabled and organized by Projekt DEAL.

Conflict of Interest

The authors declare no conflict of interest.

Keywords: ground states · hemithioindigo · molecular motors · photochemistry · rotation mechanisms

[1] a) E. R. Kay, D. A. Leigh, F. Zerbetto, *Angew. Chem. Int. Ed.* **2007**, *46*, 72–191; *Angew. Chem.* **2007**, *119*, 72–196; b) S. Kassem, T. van Leeuwen, A. S. Lubbe, M. R. Wilson, B. L. Feringa, D. A. Leigh, *Chem. Soc. Rev.* **2017**, *46*, 2592–2621; c) D. Roke, S. J. Wezenberg, B. L. Feringa, *Proc. Natl. Acad. Sci. USA* **2018**, *115*, 9423–9431; d) M. Baroncini, S. Silvi, A. Credi, *Chem. Rev.* **2020**, *120*, 200–268; e) V. Garcia-Lopez, D. Liu, J. M. Tour, *Chem. Rev.* **2020**, *120*, 79–124.

[2] a) H. A. Kistemaker, P. Stacko, J. Visser, B. L. Feringa, *Nat. Chem.* **2015**, *7*, 890–896; b) S. Erbas-Cakmak, D. A. Leigh, C. T. McTernan, A. L. Nussbaumer, *Chem. Rev.* **2015**, *115*, 10081–10206; c) M. J. Barrell, A. G. Campana, M. von Delius, E. M. Geertsema, D. A. Leigh, *Angew. Chem. Int. Ed.* **2011**, *50*, 285–290; *Angew. Chem.* **2011**, *123*, 299–304; d) D. Roke, M. Sen, W. Danowski, S. J. Wezenberg, B. L. Feringa, *J. Am. Chem. Soc.* **2019**, *141*, 7622–7627; e) M. Guentner, M. Schildhauer, S. Thumser, P. Mayer, D. Stephenson, P. J. Mayer, H. Dube, *Nat. Commun.* **2015**, *6*, 8406; f) R. Wilcken, M. Schildhauer, F. Rott, L. A. Huber, M. Guentner, S. Thumser, K. Hoffmann, S. Oesterling, R. de Vivie-Riedle, E. Riedle, H. Dube, *J. Am. Chem. Soc.* **2018**, *140*, 5311–5318; g) L. A. Huber, K. Hoffmann, S. Thumser, N. Böcher, P. Mayer, H. Dube, *Angew. Chem. Int. Ed.* **2017**, *56*, 14536–14539; *Angew. Chem.* **2017**, *129*, 14728–14731; h) A. Gerwien, P. Mayer, H. Dube, *J. Am. Chem. Soc.* **2018**, *140*, 16442–16445; i) M. Schildhauer, F. Rott, S. Thumser, P. Mayer, R. de Vivie-Riedle, H. Dube, *ChemPhotoChem* **2019**, *3*, 365–371; j) A. Gerwien, P. Mayer, H. Dube, *Nat. Commun.* **2019**, *10*, 4449; k) N. Koumura, R. W. J. Zijlstra, R. A. van Delden, B. L. Feringa, *Nature* **1999**, *401*, 152–155; l) L. Greb, J. M. Lehn, *J. Am. Chem. Soc.* **2014**, *136*, 13114–13117.

[3] P. Štacko, J. C. M. Kistemaker, T. van Leeuwen, M.-C. Chang, E. Otten, B. L. Feringa, *Science* **2017**, *356*, 964–968.

[4] a) E. Uhl, S. Thumser, P. Mayer, H. Dube, *Angew. Chem. Int. Ed.* **2018**, *57*, 11064–11068; *Angew. Chem.* **2018**, *130*, 11231–11235; b) E. Uhl, P. Mayer, H. Dube, *Angew. Chem. Int. Ed.* **2020**, *59*, 5730–5737; *Angew. Chem.* **2020**, *132*, 5779–5786.

[5] a) Q. Li, G. Fuks, E. Moulin, M. Maaloum, M. Rawiso, I. Kulic, J. T. Foy, N. Giuseppone, *Nat. Nanotechnol.* **2015**, *10*, 161–165; b) J. T. Foy, Q. Li, A. Goujon, J.-R. Colard-Itte, G. Fuks, E. Moulin, O. Schiffmann, D. Dattler, D. P. Funeriu, N. Giuseppone, *Nat. Nanotechnol.* **2017**, *12*, 540–545; c) J. Chen, F. K. Leung, M. C. A. Stuart, T. Kajitani, T. Fukushima, E. van der Giessen, B. L. Feringa, *Nat. Chem.* **2018**, *10*, 132–138.

[6] a) D. Roke, C. Stuckhardt, W. Danowski, S. J. Wezenberg, B. L. Feringa, *Angew. Chem. Int. Ed.* **2018**, *57*, 10515–10519; *Angew. Chem.* **2018**, *130*, 10675–10679; b) T. van Leeuwen, W. Danowski, S. F. Pizzolato, P. Stacko, S. J. Wezenberg, B. L. Feringa, *Chem. Eur. J.* **2018**, *24*, 81–84; c) S. J. Wezenberg, B. L. Feringa, *Nat. Commun.* **2018**, *9*, 1984; d) J. Bauer, L. Hou, J. C. Kistemaker, B. L. Feringa, *J. Org. Chem.* **2014**, *79*, 4446–4455; e) A. A. Kulago, E. M. Mes, M. Klok, A. Meetsma, A. M. Brouwer, B. L. Feringa, *J. Org. Chem.* **2010**, *75*, 666–679; f) T. van Leeuwen, A. S. Lubbe, P. Štacko, S. J. Wezenberg, B. L. Feringa, *Nat. Chem. Rev.* **2017**, *1*.

[7] a) J. Wang, B. L. Feringa, *Science* **2011**, *331*, 1429–1432; b) D. Zhao, T. M. Neubauer, B. L. Feringa, *Nat. Commun.* **2015**, *6*, 6652; c) S. F. Pizzolato, P. Stacko, J. C. M. Kistemaker, T. van Leeuwen, E. Otten, B. L. Feringa, *J. Am. Chem. Soc.* **2018**, *140*, 17278–17289; d) S. F. Pizzolato, P. Štacko, J. C. M. Kistemaker, T. van Leeuwen, B. L. Feringa, *Nat. Catal.* **2020**, *3*, 488–496; e) K. Grill, H. Dube, *J. Am. Chem. Soc.* **2020**, *142*, 19300–19307.

[8] a) L. Greb, A. Eichhofer, J. M. Lehn, *Angew. Chem. Int. Ed.* **2015**, *54*, 14345–14348; *Angew. Chem.* **2015**, *127*, 14553–14556; b) J. Wang, B. Durbeej, *ChemistryOpen* **2018**, *7*, 583–589; c) B. Oruganti, J. Wang, B. Durbeej, *Int. J. Quantum Chem.* **2018**, *118*, e25405; d) C. Garcia-Iriepa, M. Marazzi, F. Zapata, A. Valentini, D. Sampedro, L. M. Frutos, *J. Phys. Chem. Lett.* **2013**, *4*, 1389–1396; e) G. Ragazzon, M. Baroncini, S. Silvi, M. Venturi, A. Credi, *Nat. Nanotechnol.* **2015**, *10*, 70–75; f) J. V. Hernandez, E. R. Kay, D. A. Leigh, *Science* **2004**, *306*, 1532–1537; g) G. B. Boursalian, E. R. Nijboer, R. Dorel, L. Pfeifer, O. Markovitch, A. Blokhuis, B. L. Feringa, *J. Am. Chem. Soc.* **2020**, *142*, 16868–16876.

[9] a) V. Garcia-Lopez, F. Chen, L. G. Nilewski, G. Duret, A. Aliyan, A. B. Kolomeisky, J. T. Robinson, G. Wang, R. Pal, J. M. Tour, *Nature* **2017**, *548*, 567–572; b) A. S. Lubbe, Q. Liu, S. J. Smith, J. W. de Vries, J. C. M. Kistemaker, A. H. de Vries, I. Faustino, Z. Meng, W. Szymanski, A. Herrmann, B. L. Feringa, *J. Am. Chem. Soc.* **2018**, *140*, 5069–5076; c) R. S. Gunasekera, T. Galbadage, C. Ayala-Orozco, D. Liu, V. Garcia-Lopez, B. E. Troutman, J. J. Tour, R. Pal, S. Krishnan, J. D. Cirillo, J. M. Tour, *ACS Appl. Mater. Interfaces* **2020**, *12*, 13657–13670.

[10] a) C. Petermayer, H. Dube, *Acc. Chem. Res.* **2018**, *51*, 1153–1163; b) S. Wiedbrauk, H. Dube, *Tetrahedron Lett.* **2015**, *56*, 4266–4274.

[11] a) P. Friedländer, *Chem. Ber.* **1906**, *39*, 1060–1066; b) V. A. Izmail'skii, M. A. Mostoslavskii, *Ukr. Khem. Zh.* **1961**, *27*, 234–237; c) T. Cordes, T. Schadendorf, K. Rück-Braun, W. Zinth, *Chem. Phys. Lett.* **2008**, *455*, 197–201; d) F. F. Graupner, T. T. Herzog, F. Rott, S. Oesterling, R. de Vivie-Riedle, T. Cordes, W. Zinth, *Chem. Phys.* **2018**, *515*, 614–621.

[12] R. Wilcken, L. Huber, K. Grill, M. Guentner, M. Schildhauer, S. Thumser, E. Riedle, H. Dube, *Chem. Eur. J.* **2020**, *26*, 13507–13512.

Manuscript received: March 15, 2021
Accepted manuscript online: May 4, 2021
Version of record online: June 4, 2021

